Polymorphism and Electrical Properties in the New Oxide $Bi_6Mo_2O_{15}$

E. Vila, J. M. Rojo, J. E. Iglesias, and A. Castro*

Instituto de Ciencia de Materiales de Madrid, CSIC, Cantoblanco, 28049 Madrid, Spain

Received December 17, 2003. Revised Manuscript Received February 16, 2004

A new oxide of composition $Bi_6Mo_2O_{15}$ has been isolated in the binary system Bi_2O_3−MoO_3. A wet-chemistry procedure, different from coprecipitation, has been used to prepare a nanosized, very reactive precursor. Annealing at different temperatures and for different time lengths leads to isolated polycrystalline polymorphs. X-ray powder diffraction studies on the hitherto unknown low-temperature form, L-$Bi_6Mo_2O_{15}$, show that it crystallizes in the monoclinic system, with unit-cell parameters a = 29.0674(5) Å, b = 5.64795(7) Å, c = 8.6620(1) Å, β = 97.979(1)°, and V = 1408.3 Å^3. The high-temperature polymorph, H-$Bi_6Mo_2O_{15}$, belongs to the well-known $[Bi_{12}O_{14}]$ columnar structural type. The relationship between the unit-cell parameters of both phases points at the connection of their structural frameworks. Impedance spectroscopy measurements show that the transition L↔H-$Bi_6Mo_2O_{15}$ is partially reversible, as well as the existence of a second high-temperature phase H′, similar to H. In contrast, the transition H→H′-$Bi_6Mo_2O_{15}$ is not reversible. These materials turn out to be good ionic conductors, with conductivities in the order L < H < H′ for all temperatures tested.

Introduction

Mixed oxides belonging to the binary system Bi_2O_3−MoO_3 have attracted much attention for several years because of the wide range of useful properties exhibited. Particularly, they are used as very effective catalysts in the partial oxidation of olefins to produce unsaturated aldehydes, unsaturated nitrides, or dienes.[1−4] Furthermore, some of the mixed oxides of bismuth and molybdenum have been revealed as good ionic conductors[5−11] and, for this reason, a renewed interest on their study has taken place. Many phases are known in this system: $Bi_{14}MoO_{24}$,[12] $Bi_{0.84}Mo_{0.16}O_{1.74}$,[13] $Bi_{38}Mo_7O_{78}$,[14,15] Bi_2MoO_6 (γ-phase),[16] $Bi_{26}Mo_{10}O_{68.5+\delta}$,[17,18] $Bi_2Mo_2O_9$ (β-phase),[19] and $Bi_2Mo_3O_{12}$ (α-phase).[20] It is worthwhile noting that these phases can all be related to the fluorite structure,[21] which is known to favor high ionic conductivity.[22] The only exception to this structural relationship is the low-temperature form γ(L)-Bi_2MoO_6,[23] which exhibits a layered Aurivillius-like structure with $[Bi_2O_2]$ sheets alternating with $[MoO_4]$ slabs in one crystallographic direction.

Perhaps $Bi_{26}Mo_{10}O_{68.5+\delta}$ is one of the most complicated phases belonging to this system because it represents a solid solution with limits placed around xBi_2O_3:MoO_3, 1.3 ≤ x ≤ 1.7. In fact, there is a widespread controversy over the precise position of these limits: while all authors seem to approximately agree with the lower limit, Galy et al.[10] claim that the upper limit must be situated at $x \approx 1.75$, in contrast to Vannier et al.[5,24] and Buttrey et al.,[17] who think it must be limited to $x \approx 1.4$. The framework of these phases is built up from $[Bi_{12}O_{14}]$ columns, extending along one prominent crystallographic direction, surrounded by $[BiMo_4O_{16}]$ entities and isolated MoO_4 tetrahedra. Its

* Corresponding author. Tel.: (+34) 91 334 9000. Fax: (+34) 91 372 0623. E-mail: acastro@icmm.csic.es.

(1) Egashira, M.; Matsuo, K.; Kagawa, S.; Seiyama, T. *J. Catal.* **1979**, *58*, 409.
(2) Brazdil, J. F.; Suresh, D. D.; Grasselli, R. K. *J. Catal.* **1980**, *66*, 347.
(3) Galvan, D. H.; Fuentes, S.; Avalos-Borja, M.; Cota-Araiza, L.; Early, E. A.; Maple, M. B.; Cruz-Reyes, J. *J. Phys. Condens. Matter* **1993**, *5*, A217.
(4) Agarwal, D. D.; Madhok, K. L.; Goswami, H. S. *React. Kinet. Catal. Lett.* **1994**, *52*, 225.
(5) Vannier, R. N.; Mairesse, G.; Abraham, F.; Nowogrocki, G. *J. Solid State Chem.* **1996**, *122*, 394.
(6) Vannier, R. N.; Danzé, S.; Nowogrocki, G.; Huvé, M.; Mairesse, G. *Solid State Ionics* **2000**, *136*−*137*, 51.
(7) Sim, L. T.; Lee, C. K.; West, A. R. *J. Mater. Chem.* **2002**, *12*, 17.
(8) Fafilek, G.; Kurek, P. *Solid State Ionics* **2003**, *157*, 171.
(9) Bastide, B.; Enjalbert, R.; Salles, P.; Galy, J. *Solid State Ionics* **2003**, *158*, 351.
(10) Galy, J.; Enjalbert, R.; Rozier, P.; Millet, P. *Solid State Sci.* **2003**, *5*, 165.
(11) Bégué, P.; Rojo, J. M.; Enjalbert, R.; Galy, J.; Castro, A. *Solid State Ionics* **1998**, *112*, 275.
(12) Crumpton, T. E.; Francesconi, M. G.; Greaves, C. *J. Solid State Chem.* **2003**, *175*, 197.
(13) Valldor, M.; Esmaeilzadeh, S.; Pay-Gomez, C.; Grins, J. *J. Solid State Chem.* **2000**, *152*, 573.
(14) Buttrey, D. J.; Jefferson, D. A.; Thomas, J. M. *Mater. Res. Bull.* **1986**, *21*, 739.
(15) Spinolo, G.; Tomasi, C. *Powder Diffr.* **1997**, *12*, 16.
(16) Kohlmuller, R.; Badaud, J. P. *Bull. Soc. Chim. Fr.* **1969**, *10*, 3434.
(17) Buttrey, D. J.; Vogt, T.; Yap, G. P. A.; Rheingold, A. L. *Mater. Res. Bull.* **1997**, *32*, 947.
(18) Enjalbert, R.; Hasselmann, G.; Galy, J. *J. Solid State Chem.* **1997**, *131*, 236.
(19) Chen, H.-Y.; Sleight, A. W. *J. Solid State Chem.* **1986**, *63*, 70.
(20) Theobald, F.; Laarif, A.; Hewat, A. W. *Mater. Res. Bull.* **1985**, *20*, 653.
(21) Buttrey, D. J.; Jefferson, D. A.; Thomas, J. M. *Philos. Mag. A* **1986**, *53*, 897.
(22) Shuk, P.; Wiemhofer, H.-D.; Guth, U.; Gopel, W.; Greenblatt, M. *Solid State Ionics* **1993**, *89*, 179.
(23) Buttrey, D. J.; Vogt, T.; Wildgruber, U.; Robinson, W. R. *J. Solid State Chem.* **1994**, *111*, 118.
(24) Vannier, R. N.; Mairesse, G.; Abraham, F.; Nowogrocki, G. *J. Solid State Chem.* **1999**, *142*, 294.

10.1021/cm035336x CCC: $27.50
Published on Web 03/20/2004

main interest, in addition to the unusual structural arrangement, appears to be centered on the important electrical properties, representing a new family of oxide conductors.

Other oxide families showing a structure with the same $[Bi_{12}O_{14}]$ columns are the high-temperature polymorph γ(H)-Bi_2MoO_6 and its isostructural compounds obtained by substituting with lone-pair active cations for Bi^{3+}, $Bi_{2-y}M_yMoO_6$ ($M = Sb^{3+}$, As^{3+}),[25,26] and the oxide recently reported $Bi_6Cr_2O_{15}$,[27,28] where the $[Bi_{12}O_{14}]$ columns are only surrounded by isolated CrO_4 tetrahedra. All these oxides are more or less good ionic conductors.

In view of this, it seems reasonable to search for new phases in the system $Bi_2O_3-MoO_3$, with well-defined compositions, hopefully belonging to the $[Bi_{12}O_{14}]$ columnar structural type, with the aim of improving the electrical response of these materials. Thus, the authors have undertaken the synthesis and study of the oxide $Bi_6Mo_2O_{15}$, analogous to $Bi_6Cr_2O_{15}$, whose existence was long ago indicated by Egashira et al.[1] in two possible forms of low and high temperature. These phases were not structurally characterized, nor were they studied from the point of view of their electrical behavior.

This work reports on the synthesis, by a new wet-chemistry method, different from coprecipitation, of two polymorphic phases of $Bi_6Mo_2O_{15}$ composition, as well as on their thermal behavior, structural characterization, and electrical response. A tentative relationship between structure and electrical properties is put forward.

Experimental Section

The so-called *n*-butylamine procedure[29,30] has been employed for the synthesis of reactive precursors of $Bi_6Mo_2O_{15}$ oxide. This precursor was prepared by adding the amount of MoO_3 (Merck, analytical grade) required to obtain a Bi:Mo molar ratio of 3:1 to 0.03 mol of $Bi(NO_3)_3{\cdot}5H_2O$ dissolved in 10 mL of HNO_3 (65% concentration), to which 200 mL of distilled water was added, under continuous stirring. The precursor material was obtained by precipitation of Bi^{3+} cation with slow addition (2 mL min^{-1}) of 1 M solution of *n*-butylamine at room temperature, with continuous stirring up to pH ~ 9.5. Then, this suspension was filtered, and the precipitate was washed with distilled water and dried at 80 °C. The composition of the mother liquid was analyzed by ICP (inductively coupled plasma) emission spectroscopy, using a Perkin-Elmer Plasma 40. The solid precursor was annealed at increasing temperatures, for different lengths of time, to the complete formation of single phases. Each treatment was finished by slow cooling within the furnace.

The evolution of the reactions was followed by X-ray powder diffraction (XRD) on a Philips X'Pert diffractometer, fitted with a Ge(111) incident beam monochromator of the Johansson symmetric type, using Cu $K\alpha_1$ radiation ($\lambda = 1.5405981$ Å). Data were recorded between 5 and 70° (2θ), with 2θ increments of 0.02° and counting time of 1 s per step. For the determination of the lattice parameters, patterns from 5 to 69° (2θ) were measured at 22 °C in the same Philips X'Pert diffractometer. The data were taken with a 0.125° divergence slit, an antiscatter slit of 1°, a receiving slit of 0.1 mm, and a set of Soller slits with an axial divergence of ≈1.1° in the diffracted beam path. The usual $\theta/2\theta$ mode was used, and intensity was counted at steps of 0.01° for 35 s. The flat sample was spun around its normal at about 2 Hz. A second trace was obtained under the same conditions and reduced 2θ domain, with a small amount of NIST Si standard (Standard Reference Material 640b, $a = 5.430940$ Å for the wavelength quoted above) mixed with the sample material, for calibration purposes. Peak positions were determined by hand, with the help of software developed by one of us (E. Vila).

The thermal behavior of different samples was studied by thermogravimetric (TG) and differential thermal analysis (DTA). The DTA and TG measurements were carried out in air, from room temperature to 850 °C, using a Seiko 320 instrument, with α-Al_2O_3 as the inert reference material. The heating−cooling rates were 10 °C min^{-1} and the quantity of sample used was about 37 mg. The evolved gases were analyzed with a Pfeiffer mass spectrometer, ThermoStar GSD 301T, with Ar as gas carrier, to determine the molecular mass.

The determination of the volumic mass of the new isolated phase was carried out with an Accupyc 1330 pycnometer using the helium displacement technique.

The particle morphology of the precursor and annealed samples were investigated by scanning electron microscopy (SEM). The images were taken in the range of 10−20 kV in a digital scanning microscope DSM 960 Zeiss. For this purpose, dispersed particles were placed on a carbon film and a gold layer was sputtered onto the powder samples.

Electrical conductivity measurements of $Bi_6Mo_2O_{15}$ were carried out by complex impedance spectroscopy with an 1260 Solartron impedance/gain-phase analyzer. Pellets of about 6-mm diameter and 1.5-mm thickness were prepared by cold pressing (1000 kg cm^{-2}) of each phase. The pellets were sintered at 675, 845, or 880 °C for 12 h, depending on the polymorphic phase to be studied, and slowly cooled to room temperature. The density of these pellets, relative to the theoretical density, was 79%, 80%, and 86%, respectively. Platinum electrodes on the two faces of the pellets were obtained by application of a Pt (Engelhard 6082) paste that was heated at 300 °C for 3 h and then at each temperature of sintering for 3 more hours. The measurements were carried out in the temperature range 200−825 °C, in steps of 25 °C, at steady temperatures, with pellets under airflow. The frequency range was $5-10^6$ Hz.

Results and Discussion

The XRD pattern of the precursor obtained by the *n*-butylamine method is shown in Figure 1 (RT). It presents the diffraction lines characteristic of a very oriented MoO_3 crystalline phase, suggesting that the structure of this oxide was not affected, while the broad band, typical of amorphous phases, indicates the presence of the bismuth component. The composition of this precursor keeps well the Bi/Mo = 3/1 relation since traces of neither cation were detected by ICP analysis in the separated mother liquid.

The TG curve of the precursor displayed, on heating, three weight-loss steps (Figure 2a): 2.9 wt % between room temperature and 335 °C; 2.2 wt % from 335 to 460 °C; and 2.8 wt % between 460 and 580 °C. These effects correlated with the respective endothermic processes observed in the DTA curve, where two additional effects appeared, the first one, a very sharp endothermic peak, centered at 650 °C and the second one, broad and not well-defined, is located between 685 and 700 °C. It is

(25) Bégué, P.; Enjalbert, R.; Galy, J.; Castro, A. *Solid State Sci.* **2000**, *2*, 637.
(26) Bégué, P.; Enjalbert, R.; Castro, A. *J. Solid State Chem.* **2001**, *159*, 72.
(27) Grins, J.; Esmaeilzadeh, S.; Hull, S. *J. Solid State Chem.* **2002**, *163*, 144.
(28) Bégué, P.; Rojo, J. M.; Iglesias, J. E.; Castro, A. *J. Solid State Chem.* **2002**, *166*, 7.
(29) Martín de Vidales, J. L.; Rojas, R. M.; Vila, E.; García-Martínez, O. *Mater. Res. Bull.* **1994**, *29*, 1163.
(30) Lisoni, J. G.; Millán, P.; Vila, E.; Martín de Vidales, J. L.; Hoffmann, T.; Castro, A. *Chem. Mater.* **2001**, *13*, 2084.

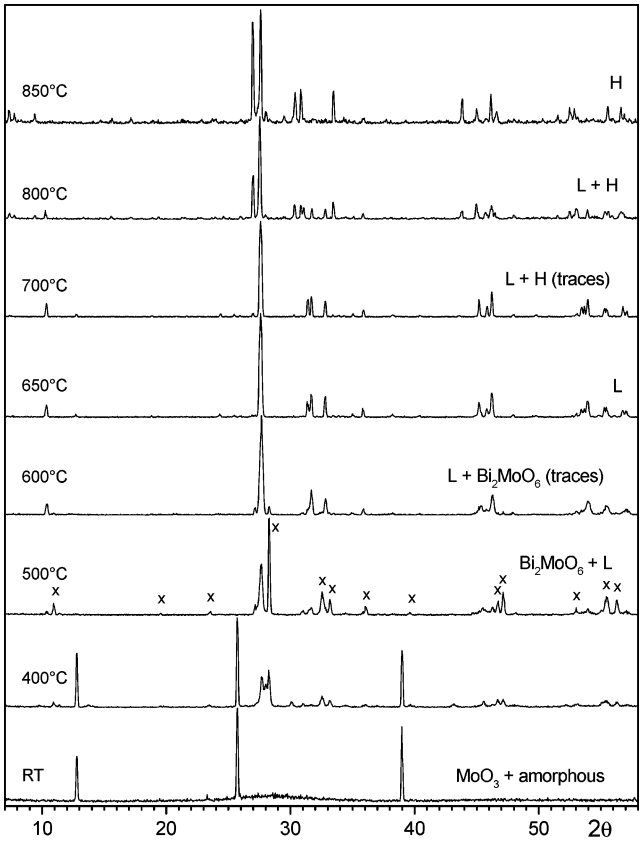

Figure 1. XRD patterns of the precursor of $Bi_6Mo_2O_{15}$ treated for 2 h at increasing temperatures. (RT = room temperature; $x = \gamma$(L)-Bi_2MoO_6; L = L-$Bi_6Mo_2O_{15}$; H = H-$Bi_6Mo_2O_{15}$).

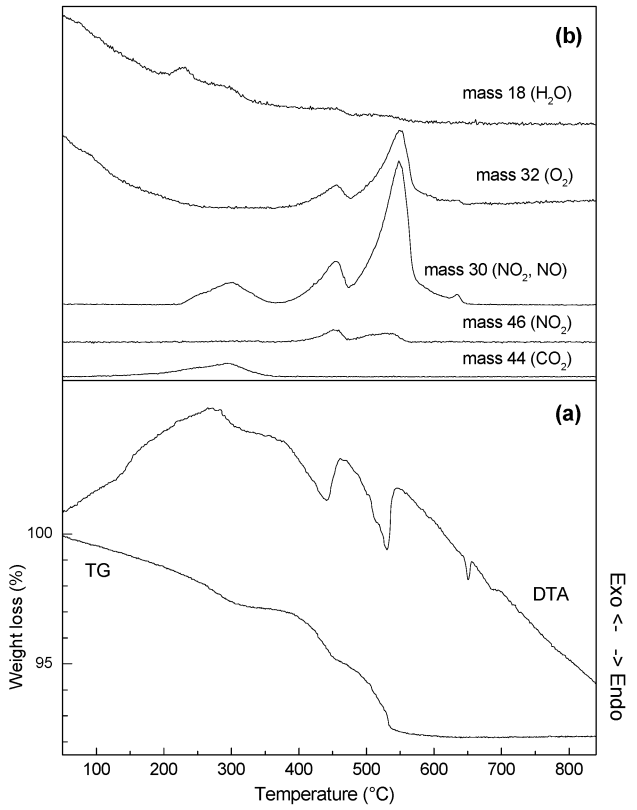

Figure 2. Thermal behavior of the precursor of $Bi_6Mo_2O_{15}$ on heating: (a) TG/DTA tracings and (b) mass spectra corresponding to the evolved gases H_2O, CO_2, O_2, NO, and NO_2.

noticeable that no effects could be observed on cooling, either in DTA or in TG. The mass spectra (Figure 2b), recorded simultaneously with the TG/DTA curves, permitted an identification of the gases evolved in each process to be made; the first mass loss was seen to correspond to the elimination of H_2O and the combustion of the organic products and evolution of CO_2 together with NO, and the last two weight losses, at temperatures higher than 335 °C, are ascribed to the elimination of O_2, NO_2, and NO.

To explain the high-temperature peaks observed in DTA, which do not correlate with weight losses, and to study the phases formed at each temperature, the precursor was annealed for 2 h at increasing temperatures, from room temperature to 850 °C, in cumulative treatments. The XRD patterns of each sample are represented in Figure 1. No structural evolution could be appreciated up to 400 °C; hence, the elimination of water and carbon oxides does not influence the arrangement of the solid phases. In contrast, from 400 to 580 °C, the elimination of nitrogen oxides strongly affect the formation of several mixed oxides of bismuth and molybdenum, probably due to the presence of amorphous $Bi(NO_3)_3$, which decomposes reacting with MoO_3. At 400 °C MoO_3 remains as a crystalline phase and the low-temperature γ(L)-Bi_2MoO_6 starts to crystallize. This phase stabilizes at 500 °C as the main crystalline phase together with a new compound (we refer to this in what follows as L-$Bi_6Mo_2O_{15}$ or L-phase) and small quantities of other oxides. At 600 °C the new oxide becomes the principal phase, and it becomes the single phase at 650 °C. Thus, the DTA endothermic peak at 650 °C can be attributed to the formation of L-$Bi_6Mo_2O_{15}$. This phase was previously detected by Egashira et al.[1] but it was not characterized. Heating at higher temperatures makes the L-phase to transform into a $[Bi_{12}O_{14}]$ columnar structure type, to be hereafter called H-$Bi_6Mo_2O_{15}$ or H-phase, that was isolated at 850 °C. So the last effect detected in DTA at about 700 °C could be due to the beginning of the structural change L→H-$Bi_6Mo_2O_{15}$. This H-phase could be considered as a member of the $[Bi_{12}O_{14}]$ columnar solid solution xBi_2O_3:MoO_3, with $x = 1.5$; this value agrees with the limits proposed by Galy et al.[10] but it is higher than the upper limit accepted by other authors.[5,17,24] We would rather not enter into a controversy about this, but our results confirm the existence of a single phase, belonging to the $[Bi_{12}O_{14}]$ columnar structural type, with composition $Bi_6Mo_2O_{15}$.

The next task was to characterize, both structurally and physically, the L- and H-$Bi_6Mo_2O_{15}$ phases. It was particularly important to isolate both oxides as pure and highly crystalline phases and to study their thermal behavior. The crystallization of the L-phase was achieved by successive heating runs of 6 h each, at 550, 600, and 625 °C, and then at increasing temperatures from 650 to 675 °C, every 5 °C, and slow cooling within the furnace, with intermediate regrinding. The XRD pattern of pure and very crystalline L-$Bi_6Mo_2O_{15}$ is shown in Figure 3a. The H-$Bi_6Mo_2O_{15}$ phase (Figure 3b) can be isolated and crystallized from the precursor sample, after a heating sequence of 10 h at 700, 835, 840 and 845 °C, respectively, with slow cooling inside the furnace and hand homogenization after each successive step. The thermal stability of this H-$Bi_6Mo_2O_{15}$ phase appears to have an upper limit: annealing at temperatures

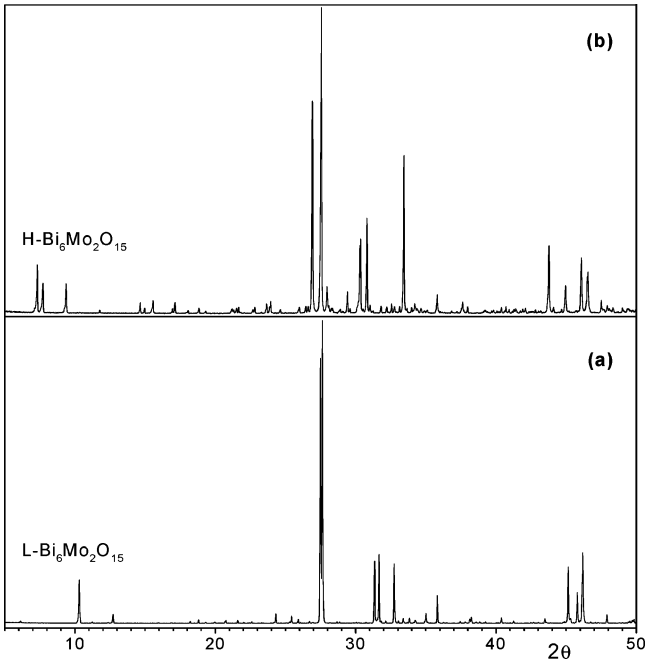

Figure 3. XRD patterns of pure phases (a) L-$Bi_6Mo_2O_{15}$ and (b) H-$Bi_6Mo_2O_{15}$.

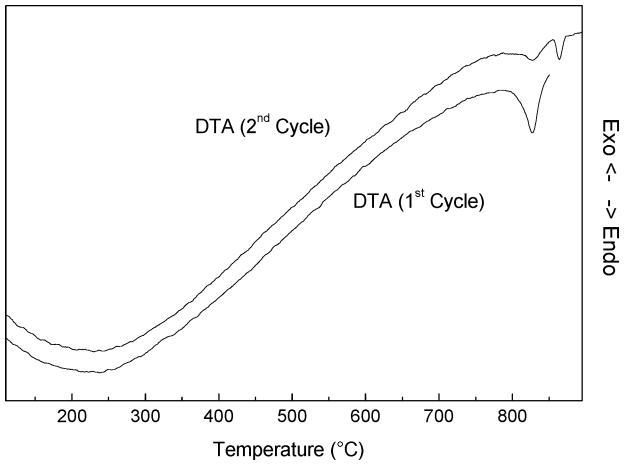

Figure 4. DTA curves on heating acquired from two consecutive heating/cooling runs, the first one up to 850 °C and the second one up to 900 °C, carried out from the L-$Bi_6Mo_2O_{15}$ oxide previously isolated.

beyond 860 °C leads to the irreversible formation of other columnar-type phases, collectively designated here as H′, which are slightly different from the H-phase, and from each other depending on the heating temperature protocol, up to the melting point at 940 °C, always with no mass loss. The formation of both H- and H′-phases can be easily observed by DTA analysis. Figure 4 depicts the DTA curves on heating, acquired from two consecutive heating/cooling cycles, the first one up to 850 °C and the second one up to 900 °C, carried out from the L-$Bi_6Mo_2O_{15}$ oxide previously isolated. The endothermic effect, centered at 827 °C in the first cycle, corresponds to the L→H transition. However, in the second run two endothermic effects can be observed, centered at 827 and 864 °C, respectively, which are attributed to the L→H transition of the remaining L-phase (827 °C), and to the H→H′ transition (864 °C). Furthermore, if room-temperature stabilized H-$Bi_6Mo_2O_{15}$ is annealed at 680 °C for 6 h, it partially reverts to L-$Bi_6Mo_2O_{15}$. These H→H+L→H transitions are depicted in Figure 5. This reversibility does not occur with the H′-phase.

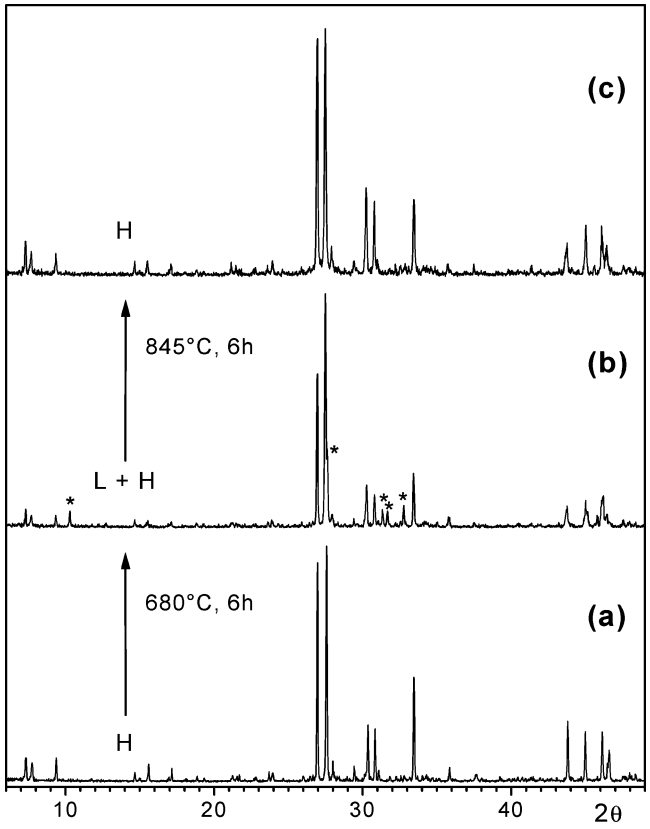

Figure 5. XRD patterns showing the H→H+L→H-$Bi_6Mo_2O_{15}$ transitions at different annealing temperatures (* = L-$Bi_6Mo_2O_{15}$).

The evolution of the grain morphology from the precursor to both L- and H-phases can be easily seen in the SEM micrographs depicted in Figure 6. The precursor sample is formed by two kinds of particles (Figure 6a), where MoO_3 appears as large crystals about 1.2 μm in size, and small spherical grains ($\approx$0.3 μm) represent the amorphous bismuth component. When this precursor is heated at 675 °C and the L-$Bi_6Mo_2O_{15}$ phase is formed, the crystal size is very much increased to 4 μm (Figure 6b), showing a quite irregular shape. Finally, the morphology of H-$Bi_6Mo_2O_{15}$ (Figure 6c), obtained at 845 °C, is different, with very large crystals exhibiting no well-defined shape; in this case the crystals can reach 20 μm in size.

Taking into account that H-$Bi_6Mo_2O_{15}$ belongs to the well-known family of compounds with general formula $M[(Bi,M')_{12}O_{14}]B_5O_{20+\delta}$[5,10,17,28,31,32] (M = Bi, Pb, Ca, Sr, Ba; M′ = Te; B = any cation in tetrahedral coordination), exhibiting a columnar structural type and crystallizing in the monoclinic system, space group *P*2/*c*, its unit-cell parameters were refined by least-squares, using our measured 2θ data and Miller indices assigned by analogy of the powder pattern with that of the model of such structures.[10] The final values of the refined lattice parameters are reported in Table 1.

(31) Enjalbert, R. Hasselmann, G.; Galy, J. *Acta Crystallogr., Sect. C: Cryst. Struct. Commun.* **1997**, *53*, 269.
(32) Castro, A.; Enjalbert, R.; Baules, P.; Galy, J. *J. Solid State Chem.* **1998**, *139*, 185.

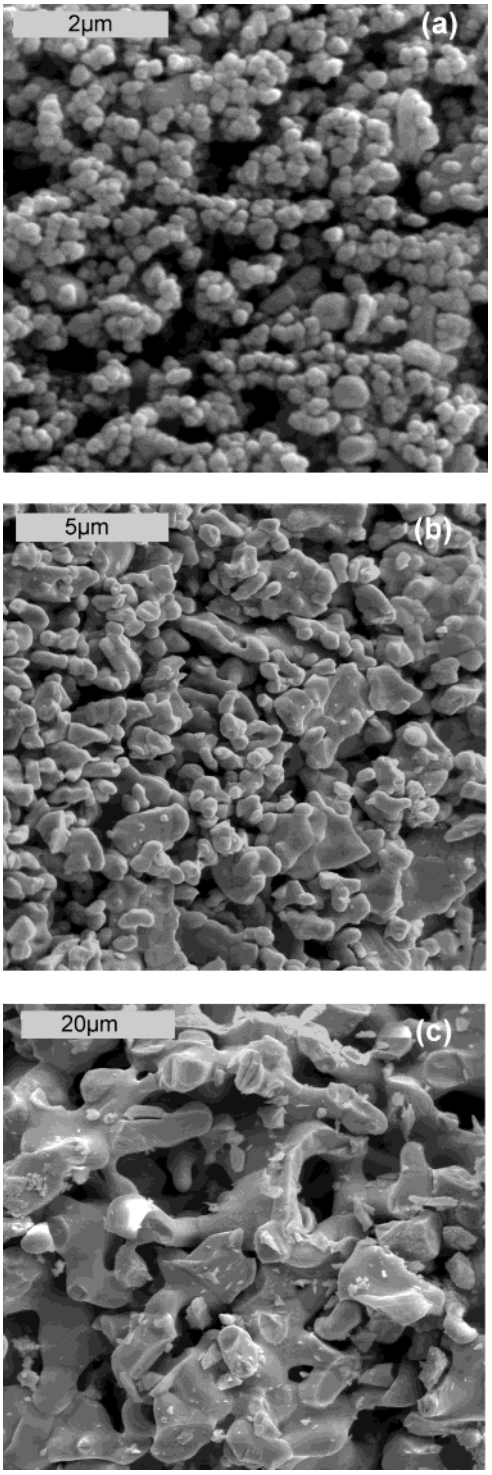

Figure 6. SEM micrographs of (a) the precursor of $Bi_6Mo_2O_{15}$, (b) L-$Bi_6Mo_2O_{15}$, and (c) H-$Bi_6Mo_2O_{15}$.

On the other hand, the L-phase has never been isolated and, hence, no structural information exists to be used as a starting point for its characterization. Therefore, an ab initio study was undertaken to determine the crystal data of L-$Bi_6Mo_2O_{15}$. The first 26 reflections of a diffractometer trace, taken under high-resolution conditions (see Experimental Section), were indexed with TREOR[33] after correction of the four lowest angle Bragg peaks with values obtained from their higher orders. A monoclinic cell with $a = 29.062$ Å, $b = 5.650$ Å, $c = 8.660$ Å, and $\beta = 97.97$ ° was found, which seemed to be a good candidate (only two extremely weak lines unindexed, M_{20}[34] = 23) for further analysis. The lattice parameters were then refined by a least-squares procedure using 166 observed lines up to $2\theta = 69°$. As the refinement advanced, it became evident that the Miller indices satisfied the selection rule: $h0l$, $h = 2n$. The rule $0k0$, $k = 2n$, is also observed, but only three reflections of this kind would be observable in the 2θ range studied. The final parameters obtained for the P-lattice of this compound were $a = 29.0674(5)$ Å, $b = 5.64795(7)$ Å, $c = 8.6620(1)$ Å, $\beta = 97.979(1)°$, and $V = 1408.3$ Å^3, with $|2\theta_{obs} - 2\theta_{cal}| \leq 0.01°$ for all observations. The density measured for this compound $\rho_{exp} = 8.01(2)$ g cm^{-3}, is in good agreement with the calculated one $\rho_x = 7.95$ g cm^{-3}, giving 4 $Bi_6Mo_2O_{15}$ formula units per cell. The final reliability estimators for this indexing were $M_{20} = 71$, ($\langle\epsilon\rangle = 0.000010$, 27); $M_{40} = 58$, ($\langle\epsilon\rangle = 0.000011$, 53); $M_{100} = 25$, ($\langle\epsilon\rangle = 0.000016$, 180); $M_{166} = 15$, ($\langle\epsilon\rangle = 0.000018$, 587). The possible space group could be any one of Pa (No. 7), $P2/a$ (No. 13), or $P2_1/a$ (No. 14). We carried out several other indexing processes, using the same initial data and different algorithms, as implemented in the suite Crysfire.[35] The above primitive monoclinic solution was obtained under several disguises (i.e., different choices of the monoclinic a and c axes) in the run of DICVOL;[36] it was also obtained as the original Niggli cell by the routine of Kohlbeck & Hörl,[37] which also reported as an orthorhombic solution the pseudo-orthorhombic ($\beta = 89.41°$) cell of double volume, which results in defining $\vec{a}' = 2\vec{a} + \vec{c}$ ($a = 57.57$ Å), $\vec{b}' = \vec{b}$, $\vec{c}' = \vec{c}$. The method of Taupin[38] was also used to exclude the possibility of any symmetry higher than monoclinic. The routine ITO[39] failed to obtain a meaningful solution. The indexed X-ray powder diffraction pattern of L-$Bi_6Mo_2O_{15}$ is reported in Table 2.

Although no information on the framework of this new oxide is available, it is worthwhile noting the existence of several features that establish a relationship between all the phases showing infinite [$Bi_{12}O_{14}$] columns in their structure and our L-$Bi_6Mo_2O_{15}$ phase. First, all phases belonging to this structural type show a small parameter, ranging from 5.57 Å for $Bi_{1.1}Sb_{0.9}MoO_6$ to 5.88 Å for $Bi_6Cr_2O_{15}$ (Table 1). This parameter represents the crystallographic direction along which the [$Bi_{12}O_{14}$] columns extend. In our case, the same parameter was found, with an intermediate value of 5.65 Å. Second, if the lone pair of electrons associated with Pb^{2+}, Bi^{3+}, Sb^{3+}, and Te^{4+} is considered to be spherically distributed, with a volume comparable with that of an oxygen ion,[40] then the average volume for each anion for all columnar structures ranges between 16.6 Å^3 for $Bi_{1.1}Sb_{0.9}MoO_6$ and 17.5 Å^3 for $PbBi_{12}Mo_5O_{34}$, with a value of 16.8 Å^3 in our case. Moreover, the

(33) Werner, P.-E.; Eriksson, L.; Westdahl, M. *J. Appl. Crystallogr.* **1985**, *18*, 367.

(34) de Wolf, P. M. *J. Appl. Crystallogr.* **1968**, *1*, 108.

(35) Shirley, R. *The Crysfire 2002 System for Automatic Powder Indexing: User's Manual*; The Lattice Press: 41 Guildford Park Avenue, Guildford, Surrey GU2 7NL, England, 2002.

(36) Boultif, A.; Louër, M. *J. Appl. Crystallogr.* **1991**, *24*, 987.

(37) Kohlbeck, F.; Hörl, E. M. *J. Appl. Crystallogr.* **1976**, *9*, 28.

(38) Taupin, D.; *J. Appl. Crystallogr.* **1973**, *6*, 380.

(39) Visser, J. W.; *J. Appl. Crystallogr.* **1969**, *2*, 89.

(40) Galy, J.; Meunier, G.; Andersson, S.; Aström, A. *J. Solid State Chem.* **1975**, *13*, 142.

Table 1. Crystal Data for Several Oxides Belonging to the $[Bi_{12}O_{14}]$ Columnar Structural Type

compound	*a* (Å)	*b* (Å)	*c* (Å)	β(°)	*V* (Å^3)	S.G.	reference
$Bi_6Cr_2O_{15}$	12.30184(5)	19.87492(7)	5.88162(2)		1438.0	*Ccc*2	26,27
L-$Bi_6Mo_2O_{15}$	29.0674(4)	5.64795(7)	8.6620(1)	97.979(1)	1408.3	*Pa*, *P*2/*a*, *P*2$_1$/*a*	this work
H-$Bi_6Mo_2O_{15}$	11.7451(9)	5.8010(4)	24.795(2)	102.910(7)	1646.7	*P*2/*c*	this work
$Bi_{26}Mo_{10}O_{69}$	11.742(8)	5.800(7)	24.77(5)	102.94(6)	1644	*P*2/*c*	5
$Bi_{13}Mo_4VO_{34}$	11.652(7)	5.7923(8)	24.420(9)	101.38(6)	1616	*P*2/*c*	17
$PbBi_{12}Mo_5O_{34}$	11.715(4)	5.800(2)	24.694(9)	102.10(3)	1641	*P*2/*c*	30
$Bi_{12}TeMo_3V_2O_{34}$	11.704(9)	5.820(1)	12.16(1)	100.90(2)	813	*P*2	31
$Bi_{11}Te_2Mo_2V_3O_{34}$	11.642(2)	5.771(1)	24.22(1)	101.16(4)	1597	*P*2/*c*	31
γ(H)-Bi_2MoO_6	17.2627(1)	22.4296(2)	5.58489(5)	90.4974(6)	2162.35	*P*2$_1$/*c*	22
$Bi_{1.1}Sb_{0.9}MoO_6$	17.0988(7)	22.3342(9)	5.5679(2)	90.926(3)	2126.0	*P*2$_1$/*c*	25

reversibility of the transition L↔H-$Bi_6Mo_2O_{15}$ encourages one to think that both scaffoldings are not very different and that this transition could be due to a topotactic rearrangement which spares the overall features of the columns. So all these facts allow us to speculate about the columnar character of the L-$Bi_6Mo_2O_{15}$ oxide also. Obviously, a complete structural study is needed to confirm or disprove this hypothesis, and this will be undertaken soon.

The impedance ($-Z''$ vs Z') plots at low temperatures (325 °C) (not shown) of the L- and H-phase consist of only one arc whose associated capacitance is 6 pF, which can be attributed to the response of the grain interior, in agreement with that usually reported.[41] The resistance has been determined from the intercept of the arc at low frequencies with the real Z' axis, and from this the corresponding conductivity has been calculated. In contrast, the impedance plots at low temperatures (200 °C) of the H′-phase show a distorted arc that seems to be formed by two overlapped arcs. The capacitance associated with the distorted arc is 14 pF, which is higher than that usually reported for the grain interior response. This fact, together with the distorted shape of the arc, seems to indicate an overlap of two responses, that of the grain interior and that of the grain boundary. In these impedance plots we have also measured the total resistance of the pellet and from this we have calculated its total conductivity.

As temperature increases from 325 to 650 °C, the impedance evolution of the plots is as follows. The high-frequency part of the arcs is progressively lost and a spike is developed at low frequencies. At high temperatures (>650 °C) the spike is bent and progressively transformed into a new arc that shows a capacitance of the order of 0.5 μF. This arc has been observed at high temperatures in ionic conductors in which oxide ions are the charge carriers.[11]

The grain interior conductivity of the L- and H-$Bi_6Mo_2O_{15}$ phases, and the total conductivity of the H′ pellet as a function of reciprocal temperature (1000/*T*), is shown in Figure 7. At temperatures below 600 °C, the experimental conductivity fits the Arrhenius equation for the three phases. However, different linear dependencies are observed. In the case of L-$Bi_6Mo_2O_{15}$ the linear dependence persists up to 650 °C where the conductivity departs from the straight line. This fact is attributed to the slow transition from L- to H-phase since both phases coexist from 650 to 825 °C. The behavior on heating of H-$Bi_6Mo_2O_{15}$ is linear up to 600 °C and yields the conductivity of this phase. Above this temperature two slope changes can be distinguished: the first one at about 625 °C and the second one at 725 °C. At 625 °C the H-phase reverts to the L-phase, as was verified by XRD. From 625 to 725 °C both L- and H-$Bi_6Mo_2O_{15}$ coexist. Finally, at very high temperature the L-phase transits, again, to the H-phase, and this explains why the conductivity is similar to the conductivity found for the L-phase at high temperatures. In summary, the conductivity measured at high temperatures, above 675 and 625 °C for the L- and H-$Bi_6Mo_2O_{15}$ phases, respectively, represents the conductivity of a mixture of both phases. In contrast, the conductivity measured at lower temperatures is that pertaining to the single phases. The activation energies of the H-phase (0.59 eV) is lower than that of the L-phase (1.20 eV).

The results obtained for the H′-phase show only linear dependencies in the whole range of temperatures analyzed. We can see two straight lines with slightly different slopes: one between 200 and 325 °C and the other in the interval from 325 to 825 °C. The change in slope can be associated with the fact that the total conductivity is due to the grain boundary conductivity plus the grain interior component. Since both conductivities are thought to operate in a series arrangement, the grain boundary contribution should be preponderant in the temperature range 200−325 °C, whereas the grain interior conductivity is likely to dominate the total conductivity at higher temperatures (325−825 °C). This interpretation explains the two straight lines found and agrees with that reported for other ceramic materials.[42] The activation energy associated with the grain boundary conductivity (0.71 eV) is slightly higher than that associated with the grain interior conductivity (0.51 eV).

Takahashi et al.[43] and Bonn et al.[44] first, and Vannier et al.[5] and Galy et al.[10] later, performed conductivity measurements on samples formulated as $Bi_6Mo_2O_{15}$, but without any distinction of the polymorphic phase studied; their synthesis temperatures and their results lead us to believe that they studied the high-temperature H′-phase, or perhaps a mixture of phases. However, no accurate results on the different polymorphic phases with $Bi_6Mo_2O_{15}$ composition have been reported until now. Comparing the conductivities of the three L-, H-, and H′-phases, one can see that, at 625 °C, H′ exhibits the highest value (8.3×10^{-3} S cm^{-1}), H an intermediate value of 1.1×10^{-3} S cm^{-1}, and L the lowest value of 6.3×10^{-5} S cm^{-1}. The maximum conductivity reached

(41) Ross Macdonald, J. *Impedance Spectroscopy. Emphasizing Solid Materials and Systems*; John Wiley and Sons: New York, 1987.

(42) Martínez-Juárez, A.; Iglesias, J. E.; Rojo, J. M. *Solid State Ionics* **1996**, *91*, 295.

(43) Takahashi, T.; Esaka, T.; Iwahawa, H. *J. Appl. Electrochem.* **1977**, *7*, 31.

(44) Boon, L.; Metselaar, R. *Solid State Ionics* **1985**, *16*, 201.

Table 2. Powder Pattern (λ = 1.5405981 Å) for L-$Bi_6Mo_2O_{15}$

	h k l	d_{obs}	I/I_0	$2\theta_{obs}$	$\Delta 2\theta$		*h k l*	d_{obs}	I/I_0	$2\theta_{obs}$	$\Delta 2\theta$
1	2 0 0	14.39	1	6.137	0.001	90	9 2 0	2.1169	1	42.677	0.000
2	0 0 1	8.58	15	10.306	0.002	91	−9 2 1	2.1006	<1	43.024	0.000
3	−2 0 1	7.86	1	11.242	0.000		8 0 3				0.009
4	2 0 1	6.95	3	12.719	0.004	92	2 0 4	2.0796	2	43.482	−0.003
5	1 1 0	5.54	<1	15.975	−0.003	93	−12 1 2	2.0740	1	43.605	−0.002
6	2 1 0	5.26	<1	16.845	−0.005	94	13 1 0	2.0616	≪1	43.880	−0.002
7	3 1 0	4.87	1	18.210	−0.002	95	−8 2 2	2.0453	<1	44.249	0.005
8	−1 1 1	4.71	1	18.808	−0.006	96	−2 1 4	2.0220	1	44.786	−0.003
9	1 1 1	4.60	<1	19.285[a]	0.003	97	−1 1 4	2.0181	1	44.877	0.003
10	−2 1 1	4.59	<1	19.335	0.002	98	−10 2 1	2.0062	20	45.158	0.003
11	−6 0 1	4.46	≪1	19.885	−0.009		−3 2 3				0.001
12	4 1 0	4.44	<1	19.965	−0.003	99	−4 1 4	1.99971	3	45.313	−0.003
13	−3 1 1	4.37	≪1	20.324	0.007	100	1 2 3	1.99118	1	45.518	−0.006
14	0 0 2	4.29	1	20.696[a]	0.004	101	−4 2 3	1.98606	<1	46.642	0.000
15	−2 0 2	4.28	1	20.757	0.001	102	12 0 2	1.97990	10	45.792	−0.002
16	3 1 1	4.11	1	21.603	0.003	103	−9 2 2	1.97171	2	45.993	−0.004
17	−4 1 1	4.09	<1	21.705	−0.001	104	2 2 3	1.96400	24	46.184	−0.003
18	5 1 0	4.03	<1	22.027	−0.002	105	−5 2 3	1.95751	1	46.346	−0.004
19	2 0 2	3.961	<1	22.426	0.008	106	−11 1 3	1.95143	<1	46.499	0.002
	6 0 1				−0.009		2 1 4				−0.001
20	−4 0 2	3.931	1	22.600	0.006	107	13 1 1	1.94807	<1	46.584	0.000
21	4 1 1	3.814	<1	23.306	0.002	108	−6 1 4	1.94181	1	46.743	−0.004
22	−5 1 1	3.793	<1	23.433	0.002	109	3 2 3	1.92900	<1	47.072	0.005
23	6 1 0	3.656	3	24.325	0.002	110	−6 2 3	1.92115	<1	47.276	0.003
24	8 0 0	3.598	<1	24.725	0.002		10 2 1				0.003
25	5 1 1	3.519	1	25.286	0.001	111	−10 2 2	1.89698	3	47.916	−0.005
26	−6 1 1	3.500	2	25.431	0.002	112	−8 1 4	1.85680	1	49.020	0.000
27	4 0 2	3.479	<1	25.585	−0.006	113	5 2 3	1.84201	1	49.440	−0.001
28	−6 0 2	3.444	1	25.852[a]	0.003	114	0 3 1	1.83884	1	49.531	0.001
29	−1 1 2	3.437	2	25.904	0.000	115	9 2 2	1.83236	1	49.718	0.008
30	0 1 2	3.415	1	26.070	0.004	116	12 2 0	1.82816	1	49.840	0.003
31	−3 1 2	3.336	1	26.702	0.006		−12 2 1				−0.006
32	6 1 1	3.242	82	27.494	0.006	117	−11 2 2	1.82248	1	50.006	0.003
33	−4 1 2	3.226	100	27.626	0.007	118	4 3 0	1.82135	1	50.039	0.000
34	8 0 1	3.166	<1	28.167	−0.004		5 1 4				0.000
35	3 1 2	3.111	1	28.674	0.004	119	−3 3 1	1.81602	<1	50.196	0.000
36	−5 1 2	3.091	1	28.858	0.001	120	3 3 1	1.79614	1	50.791	0.001
37	8 1 0	3.034	<1	29.413	0.005	121	5 3 0	1.78917	<1	51.003	0.007
38	6 0 2	2.9974	<1	29.783	0.001	122	−10 1 4	1.75533	<1	52.059	0.005
39	7 1 1	2.9888	<1	29.871	0.001	123	6 3 0	1.75251	<1	52.149	0.001
40	−8 1 1	2.9720	<1	30.043	0.004	124	5 3 1	1.73695	1	52.652[b]	−0.005
41	−6 1 2	2.9413	≪1	30.365	−0.009	125	−6 3 1	1.73441	1	52.735	0.000
42	−2 0 3	2.8817	1	31.008	0.004	126	−16 1 1	1.72555	3	53.027	−0.003
43	−10 0 1	2.8510	22	31.351	0.001	127	−2 2 4	1.71837	<1	53.266	0.000
44	0 2 0	2.8235	22	31.664	0.006	128	−3 2 4	1.71437	10	53.400	0.004
45	1 2 0	2.8105	1	31.814	0.000	129	−14 1 3	1.70744	9	53.634	0.004
46	−7 1 2	2.7823	1	32.145	0.010	130	6 3 1	1.70028	9	53.878	−0.001
47	2 0 3	2.7328	20	32.744	0.003		2 3 2				0.007
48	3 2 0	2.7090	1	33.040	0.001	131	−4 3 2	1.69815	11	53.951	−0.003
49	0 2 1	2.6820	2	33.382	0.005	132	−5 2 4	1.68901	1	54.267	0.002
	−1 2 1				−0.006		11 2 2				0.002
50	1 2 1	2.6600	1	33.667	0.003	133	14 1 2	1.68128	<1	54.537	0.004
51	6 1 2	2.6478	2	33.826	−0.001	134	−5 3 2	1.67731	<1	54.677	0.002
52	−8 1 2	2.6260	<1	34.115[a]	0.007	135	2 2 4	1.67440	2	54.780	0.002
53	−6 0 3	2.6207	1	34.186[a]	0.010		−11 2 3				0.005
54	2 2 1	2.6161	1	34.249	0.007	136	−16 1 2	1.66993	1	54.939	−0.006
55	−3 2 1	2.6129	1	34.292[b]	0.000	137	14 2 0	1.66215	8	55.218	0.003
56	−2 1 3	2.5667	1	34.929	0.007		8 1 4				−0.003
57	−10 0 2	2.5602	3	35.020	0.001	138	−2 1 5	1.65599	10	55.441	−0.002
58	3 2 1	2.5549	≪1	35.095[b]	−0.003	139	−7 2 4	1.64299	1	55.918	−0.003
59	4 0 3	2.5387	≪1	35.326	0.005	140	0 1 5	1.64159	<1	55.970	−0.001
60	1 1 3	2.5140	<1	35.685[a]	−0.002	141	16 1 1	1.63973	2	56.039	0.005
61	−4 1 3	2.5040	10	35.832	0.001		−8 0 5				−0.007
62	7 1 2	2.4955	<1	35.959	0.000	142	12 2 2	1.62112	9	56.740	0.000
63	−9 1 2	2.4747	<1	36.271	0.007	143	−8 2 4	1.61354	6	57.031	0.001
64	2 1 3	2.4598	<1	36.499	0.005	144	−2 3 3	1.57630	1	58.507	−0.006
65	12 0 0	2.3987	1	37.463	0.002	145	14 0 3	1.56931	1	58.793	−0.001
66	−6 2 1	2.3858	≪1	37.673	0.000	146	−4 3 3	1.56122	1	59.128	0.001
67	−6 1 3	2.3777	1	37.806	0.002	147	−14 1 4	1.53871	3	60.081	0.000
68	11 1 0	2.3742	<1	37.864[b]	0.004		18 1 0				0.001
69	0 2 2	2.3585	2	38.125[a]	0.002	148	8 3 2	1.52212	1	60.805	−0.008
70	−2 2 2	2.3562*	1	38.165	0.005	149	4 3 3	1.51214	1	61.249	0.007
71	8 1 2	2.3512	2	38.249	−0.004		14 1 3				−0.006
72	1 2 2	2.3363	≪1	38.502	0.000	150	−7 3 3	1.50779	<1	61.445	−0.008
73	−3 2 2	2.3320	1	38.576	0.002	151	8 2 4	1.48061	1	62.699	0.009
	−10 1 2				−0.002		18 1 1				−0.002

Table 2. (Continued)

	h k l	d_{obs}	I/I_0	$2\theta_{obs}$	$\Delta 2\theta$		*h k l*	d_{obs}	I/I_0	$2\theta_{obs}$	$\Delta 2\theta$
74	7 2 0	2.3279	<1	38.646	0.000	152	−12 1 5	1.44729	<1	64.313	−0.001
75	6 0 3	2.3187	<1	38.807	0.002	153	−20 0 2	1.42548	2	65.419	0.002
76	4 1 3	2.3162	1	38.850	−0.006		−6 0 6				−0.005
77	−7 1 3	2.2994	<1	39.145[a]	−0.005	154	8 1 5	1.42393	1	65.499	−0.008
	6 2 1				−0.004	155	−2 3 4	1.42075	<1	65.664	0.000
78	−4 2 2	2.2943	1	39.235	−0.010	156	−8 2 5	1.41799	2	65.808	−0.005
79	−7 2 1	2.2923	1	39.272	0.007	157	0 4 0	1.41188	2	66.129	0.006
80	10 0 2	2.2500	<1	40.041	0.001	158	−16 2 3	1.41039	<1	66.208	0.003
81	−5 2 2	2.2432	<1	40.168	0.006		1 4 0				−0.005
82	12 0 1	2.2312	2	40.392	0.000	159	4 2 5	1.40447	1	66.523	0.002
83	8 2 0	2.2219	<1	40.569	−0.008	160	−2 1 6	1.39767	2	66.889	−0.001
84	9 1 2	2.2156	<1	40.689[c]	0.001	161	2 4 1	1.38381	1	67.649	−0.002
85	−12 1 1	2.2074	≪1	40.847	0.000	162	14 2 3	1.37177	1	68.324	−0.003
86	−11 1 2	2.1980	<1	41.031	0.000	163	4 0 6	1.36642	2	68.629	0.005
87	−10 0 3	2.1858	1	41.269	0.004	164	12 3 2	1.36433	1	68.749	−0.002
88	0 0 4	2.1443	<1	42.105	0.004	165	−12 3 3	1.36374	<1	68.783	−0.004
89	5 2 2	2.1265	<1	42.475	−0.003	166	4 4 1	1.36207	<1	68.879	0.003
	−9 1 3				0.009						

[a] Shoulder of following. [b] Shoulder of precedent. [c] Incompletely resolved from precedent.

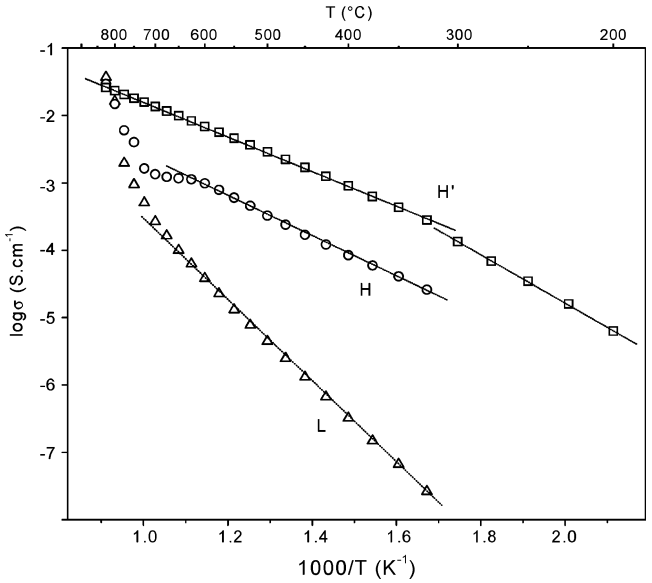

Figure 7. Conductivity (σ) versus reciprocal temperature for L-, H-, and H′-$Bi_6Mo_2O_{15}$ phases.

by the single L- and H′-phases is 1.0×10^{-4} S cm^{-1} at 650 °C and 2.6×10^{-2} S cm^{-1} at 825 °C, respectively.

In the temperature range studied, the materials exhibit quite good characteristics as ionic conductors, as compared with other phases also exhibiting columnar-type structures. Thus, the H′-phase shows a higher conductivity than that of $Bi_{26}Mo_{10}O_{69}$, and a conductivity similar to that of the best ionic conductor of this family, $Bi_{26}Mo_8Cr_2O_{69}$.[28] On the other hand, H-$Bi_6Mo_2O_{15}$ is a conductor better than $Pb_2Bi_{24}Mo_{10}O_{69}$, but similar to $Bi_{26}Mo_8V_2O_{68}$, $Bi_{24}Te_2Mo_8V_2O_{68}$, and $Bi_{22}Te_4Mo_6V_4O_{68}$,[11] for example. Although L-$Bi_6Mo_2O_{15}$ is the most modest oxygen conductor of these polymorphic phases, it exhibits a higher conductivity than γ(H)-Bi_2MoO_6 does, and similar values to those shown by $Bi_6Cr_2O_{15}$.[27]

Conclusions

The soft-chemistry method reported in this work permitted us to isolate several polymorphic single phases with composition $Bi_6Mo_2O_{15}$. While the high-temperature H- and H′-phases belong to the well-known $[Bi_{12}O_{14}]$ columnar structural type and could be considered as members of the solid solution xBi_2O_3:MoO_3 ($1.3 \leq x \leq 1.7$), isostructural with the monoclinic $M[(Bi,M')_{12}O_{14}]B_5O_{20+\delta}$ oxides, the structural characteristics determined for the low-temperature L-$Bi_6Mo_2O_{15}$ show that it crystallizes in the monoclinic system, space group *Pa*, *P*2/*a*, or *P*2$_1$/*a*.

Thermal studies have demonstrated that the L-phase transforms into the H-phase at moderate temperatures, whereas H transforms irreversibly to the H′-phase at 860 °C and above and it partially reverts to the L-phase after annealing at about 650 °C.

The relationship established between the lattice parameters of all known columnar phases and L-$Bi_6Mo_2O_{15}$, as well as the reversible character of L-↔H-$Bi_6Mo_2O_{15}$ transition, point out the possible columnar character of L-phase structure.

L-, H-, and H′-phases are quite good ionic conductors, as most of the materials belonging to the $[Bi_{12}O_{14}]$ columnar structural-type.

Acknowledgment. This work was funded by projects MAT 2001-0561 and CAM 07N/0076/2002 of MCyT and CAM of Spain. SEM work has been carried out at the Centro de Ciencias Medioambientales (CSIC).

CM035336X